Jefferson Lab

Newport News, VA

GlueX/Hall D Calorimeter Final Design and Safety Review
February 19-20, 2008

Section 3:
SiPM Readout for BCAL

GlueX/Hall D Calorimeter Conceptual Design Report
Section 3 of 5

3 SiPM Development and Testing for Use for BCAL

This section reports on the status of SiPM development and testing for their use as a photo-sensor for BCAL. Jefferson Laboratory, on behalf of GlueX, contracted with SensL[1] to begin working towards a more realistic size using its patented CMOS-based technology. Testing of 12×12 mm^2 arrays is now underway at JLab and the University of Regina and is described below. Additional details can be found in a number of GlueX technical notes [1]-[10].

3.1 Testing silicon photomultipliers at JLab

3.1.1 Introduction to silicon photomultipliers

The silicon photomultiplier is an array of micro-sized (20–100 μm) avalanche photodiodes operated in Geiger mode. Each pixel has a recovery resistor associated with it to quench the resultant avalanche. In the Geiger mode, each pixel acts like a digital switch as any number of photons activating a pixel during the period of the avalanche will produce the same output as one photon. By ganging the pixels together via the associated resistors, one produces a summation device whose output is proportional to the number of detected photons.

Details of the operational characteristics of a SiPM can be found in the literature[2] [11],but some salient aspects can be noted. First, these devices have a distinct breakdown voltage under reverse bias where the probability of creating an avalanche becomes significant above this threshold. As the voltage is increased above breakdown (the overbias), the probability increases and results in an increased gain. The intrinsic gain should be linear with the overbias where typical gains are in the range of 10^5–10^6. The breakdown voltage is a function of temperature. Along with an overall lessening in noise at lower temperatures, the breakdown voltage will also decrease. The avalanche process also results in an intrinsic dark noise factor where single photoelectron pulses are created even in the complete absence of light. Furthermore, there are also events where the occurrence of a dark noise pulse can trigger a time coincident second dark noise pulse in an adjacent microcell. This is a crosstalk factor and can affect the linearity of the device. Indeed, it is creation of light by the initial avalanche that creates this secondary pulse. (In other words, this is a device that should literally "glow in the dark".) Finally, there are delayed avalanches that result in extended (over time) dark noise pulses. It is claimed that these would be more common at low temperatures [12]. Figure 3.1 is an example oscilloscope display of the dark noise pulses.

3.1.2 Testing the initial sample set

At the time when this project was begun, the standard physical size of a SiPM was 1 mm^2, although larger sizes were being developed. A 3×3 mm^2 has now become a standard size.

In order to make the final device, a square array of the 3×3 mm^2 can be used to make to 12×12 mm^2 device needed to readout each of smaller sectors. A possible goal is to produce a monolithic design with the corners omitted so as to make a better match to the circular output of the light guide.

[1] SensL, Blackrock, Cork, Ireland (**www.sensl.com**).

[2] SensL Technical Notes Library can be downloaded at **www.sensl.com.**

Figure 3.1: Oscilloscope picture of typical dark pulses in a silicon photomultiplier

Some initial studies comparing the performance of 1 mm^2 samples with traditional vacuum phototubes have been published [13]. This report concerns itself with the evaluation of the two initial sample set of 3x3 mm^2 devices. The dark noise is the usual concern when scaling up the device size since it tends to rise at least as fast as the area. Tests of 1 mm^2 samples indicated that it would be wise to include an onboard Peltier cooler. Again, initial tests indicated that an operating temperature of -20°C would be best choice for the initial evaluation tests.

Type	**No. pixels**	**Pixel size**	**Fill Factor**
C20 (1 mm^2)	620	20 μm	17.8%
C20	4496	20 μm	17.8%
A20L	6744	20 μm	34.2%
A20H	8640	20 μm	42.7%
A35L	2452	35 μm	30.5%
A50H	1930	50 μm	70.3%

Table 3.1: List of initial 3×3 mm^2 silicon pmt samples. The 1 mm^2 C20 was used as the initial room temperature reference sample.

Table 3.1 is a list of the initial samples indicating pixel size, number of pixels and the overall fill factor. (The last is the percentage of actual photosensitive surface.) One exception is the 1 mm^2 version of type C20. This had no Peltier cooler and was used in the initial tests to measure the photon detection efficiency. This initial set also included a amplifier board (gain = x21) with an additional board to control the Peltier cooler. The latter was set to produce a temperature of -20°C. The SiPM chip and cooler were mounted within a standard TO-8 can. Figure 3.2 is a picture of the system. DC power requirements were +5, -5, and a positive DC bias for the SiPM.

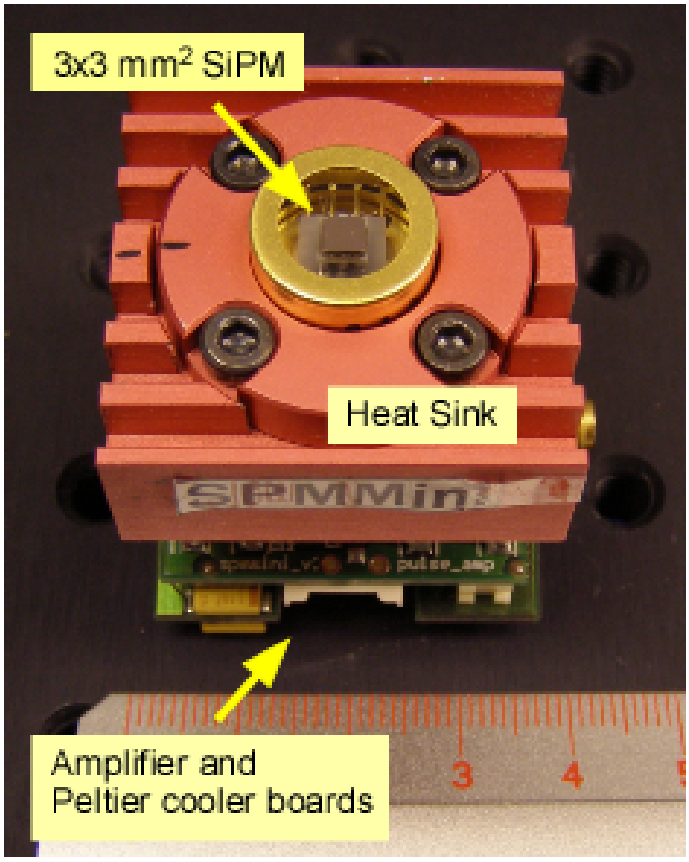

Figure 3.2: Photograph of module used to house and test SiPMs. The Peltier unit is placed directly behind the SiPM chip within the TO-8 housing.

3.1.3 Verifying photon detection efficiency

The first task was to measure the photon detection efficiency. The expression for this is the product of the following terms:

$$PDE(\lambda, \Delta V_{br}) = Q_E(\lambda) \times F \times \alpha_p(\Delta V_{br})$$

where $Q_E\,(\lambda)$ = intrinsic quantum efficiency, $\alpha_p\,(\Delta V_{br})$ = avalanche probability and F = the fraction of photosensitive surface. The parameters λ and ΔV_{br} are the wavelength and overbias (voltage above breakdown) respectively. Due to nature of the device, $Q_E \times \alpha_p$ is the actual quantity measured as α_p is proportional to the overbias voltage set for the measurement.

The initial tests of PDE were made with the 1 mm^2 C20 device (at room temperature) as this had the lowest noise level. The measurement was made in pulse mode and followed many of the principles described in reference [14]. Figure 3.3 is schematic of the basic measurement setup used for the measurements in this report. Two LEDs (blue and green) are used as pulsed light sources. Their light is delivered via a bifurcated glass fiber bundle to a beam collimation unit that creates a uniform illumination. A manual filter wheel

equipped with narrow band filters (width = 10 nm) is used to select one of two wavelengths - 450 or 520 nm. A dual set of remotely controlled filter wheels equipped with UV-VIS neutral density filters is used to control the light intensity over a broad range. One of the filter wheels controls the overall magnitude - 0, 0.1, 1, 10, or 100% while the other provides a finer control - 20, 40, 60, 80, 100%. Finally, the output light can be further diffused (and lowered in intensity) via a UV-VIS diffuser element. In this way, a large dynamic range of light intensities (including single photoelectron level) can be utilized while maintaining a highly uniform illumination of the photodetector.

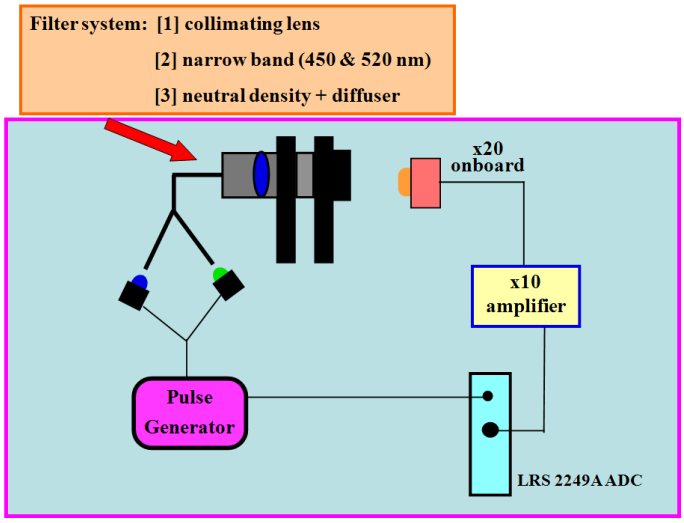

Figure 3.3: General setup for testing the SiPMs.

The measurement of the PDE involved the following prescription: 1. Use a calibrated photodiode (Hammamatsu model S2281) to calibrate the neutral density filters. 2. Given this calibration, use the photodiode to calibrate a reference PMT. 3. Using the calibrated PMT, switch to pulse mode and compare the response (at equal gain) of the PMT and SiPM at low light intensities where crosstalk effects are kept minimal.

The photodiode was used in DC mode. In this case, the LEDs were also operated in DC mode to maintain maximum stability. Using a voltage divider circuit, a current of 1 mA through the LEDs was found to be sufficient and gave a very stable output. The phototube's photocathode (XP2262) had all but a central 6 mm diameter hole masked. This allowed comparable photosensitive areas to be used and also avoided the problem of incomplete photoelectron collection efficiency across the entire 5 cm diameter surface. This phototube had been used in previous studies of PMT/base linearity and rate studies, so it was possible to gauge a range of currents that maintained linear response. A variety of intensities and distances were used to minimize systematic errors. The PDEs were determined to be (3.4±0.5)% and (4.4±0.5)% at 450 and 520 nm for an overbias of 1.2 volts and a fill factor of 18%. This was consistent with the SensL data. Their method of measurement is similar and can be found in their technical documentation.

3.1.4 SiPM gain

Measuring the PDE requires that the single photoelectron spectrum from the SiPM can be resolved to set the gain at a given overbias voltage. In subsequent work with the larger 3x3 mm^2 devices, photoelectron spectra were resolved when the devices were operated at -20°C. The noise levels were too high at room temperature to allow this possibility. Figure 3.4 shows the gain data for this set of 3x3 mm^2 devices. The

best device was the A20L for which a variety of gains were measured. This data verified that they operated at a overall gain level of 10^6 or better. Linear variation of the gain with overbias voltage was also observed. One can also see that the 35 micron microcell device produced a significantly higher intrinsic gain although a higher level of noise prevented a broad range of measurements from being made.

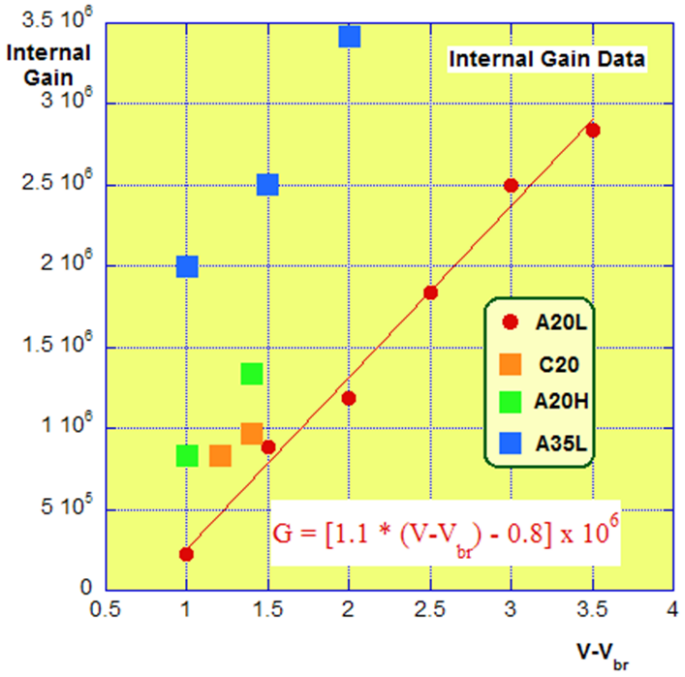

Figure 3.4: Gain data for SiPMs where the photopeaks could be resolved at -20°C. The equation is a fit for the A20L sample. Note the significantly higher gain possible with the 35 μm pixels.

3.1.5 SiPM dark noise

Noise measurements can be expressed in two ways - as a dark count rate, that is, the rate of single (and higher) photoelectron pulses, or as a DC current. The latter is often a matter of necessity if the actual count rate exceeds the capability of the instrumentation. The same can also happen if the noise level is high enough that the photoelectron peaks cannot be resolved. In this case, no plateau counting level corresponding to the single photoelectron can be found and only a smoothly falling curve in rate can be plotted.

For this set of devices, it was decided to measure the actual count rate for the A20L device at -20°C, as the photoelectron peaks could be resolved at a wide variety of gain settings. Dark current measurements would be made for all devices at both -20°C and room temperature (21°C) so as to ascertain relative differences in dark noise. The actual quantitative relationship between the two methods of measurement remains to be determined. The setup in figure is modified for measuring dark rate. The light sources are extinguished, and the dark pulses are amplified and then sent through a discriminator to create standard NIM pulses that are counted by a scalar. Due to the timing characteristic of the pulse, it was estimated that a maximum count rate of 10 MHz was quantifiable.

Figure 3.5 is the rate data for the A20L sample while Figure 3.6a) is the dark currents for all the samples. Figure 3.6b) is the dark current for the A20L sample at -20°C and room temperature. In Figure 3.6a), the

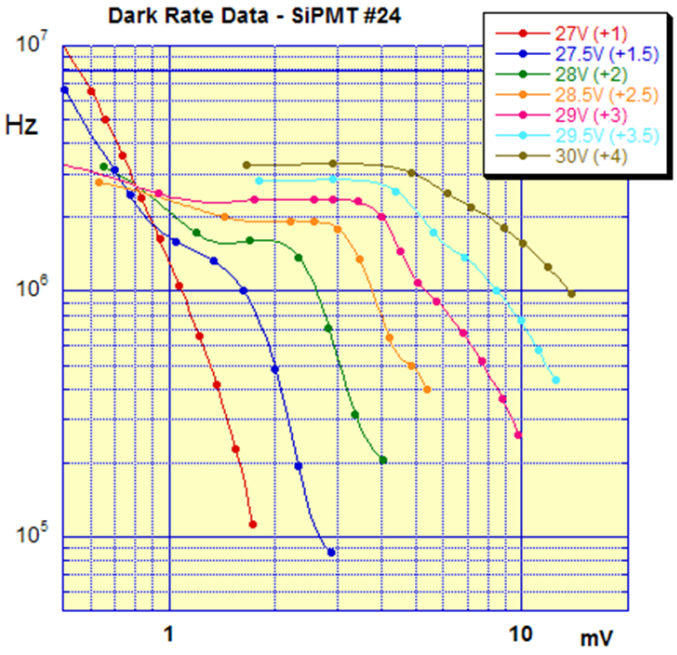

Figure 3.5: Dark rate data for the A20L sample at -20°C. The plateau is the rate of > 1 pe dark pulses. Note the unresolved data at the lowest overbias of 1 volt. The rates are consistent with what is expected for the calorimeter at room temperature.

behavior for the samples A20H and A50H was later realized to be anomalous and indicative of a problem in the device. The standard behavior is to have the dark current slowly approaching a plateau at higher voltages. The data from the cooled A20L device falls within the guidelines established for successful operation of the calorimeter. The next set of improved samples indicate that we are approaching such behavior at room temperature as is desired.

Figure 3.7 indicates another aspect of the temperature on the behavior of the SiPMs. In this case, a special circuit[3] was used where the direct output of the SiPM could be observed while allowing the temperature of the A20L device to be controlled through the included Peltier cooler. The pulse amplitude was measured at a 2V overbias as the termperature was changed from -20°C to room temperature. The measured sensitivity (2% per degree C) inidicates that even if the final device is not cooled, it will still be necessary to provide for a method of maintaining temperature stability of the device.

3.2 Latest lower noise samples

The most recent samples have been based upon several evolving improvements particularly in the noise levels. We have a set of devices based upon a A35H design (3640 pixels, 60% fill) that includes 5 samples of a 4x4 array of 3x3 mm^2 devices in a summed array (Figure 3.8). This is a first order prototype of the kind of device needed for the calorimeter. We also have a set of ten 3×3 mm^2 devices, some of which are intended for long term stability tests. Figure 3.9 shows pulses of the array in comparsion to the individual devices. For the latest A35H samples, the pulse width is too wide especially for the array. The aim is to achieve

[3]Modified circuit board provided by courtesy of Paul Smith, Department of Physics, Indiana University.

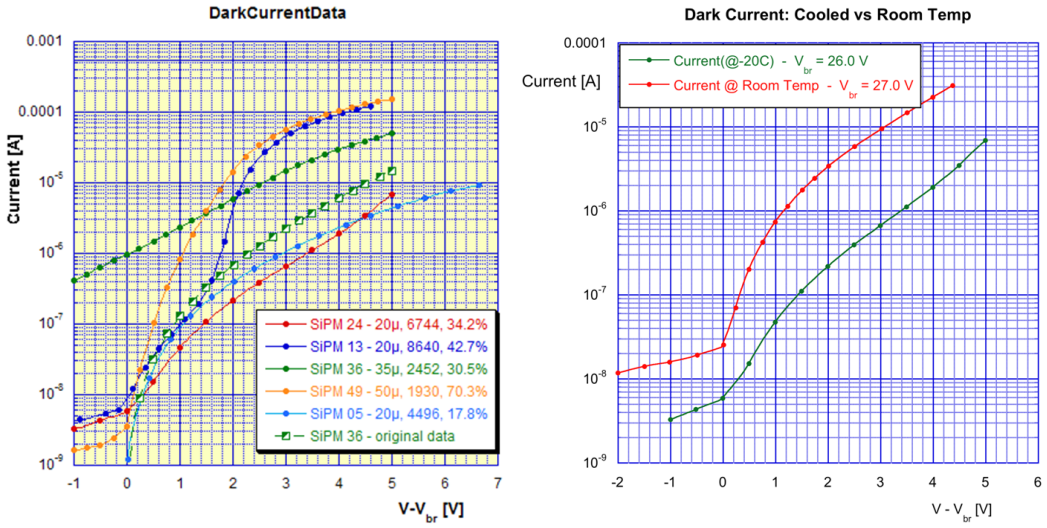

Figure 3.6: *Left panel:* a) Dark currents for the cooled SiPM samples. The 35 μm sample became unstable after about 1 day of operation and showed a substantial increase in dark current. It is now understood that samples #5 and #49 have anomalous behavior at the higher biases. *Right panel:* b) Comparison of dark current for A20L sample at -20°C and room temperature (21°C). Note the 1 volt increase in breakdown voltage. Data is presented in terms of overbias - voltage above breakdown.

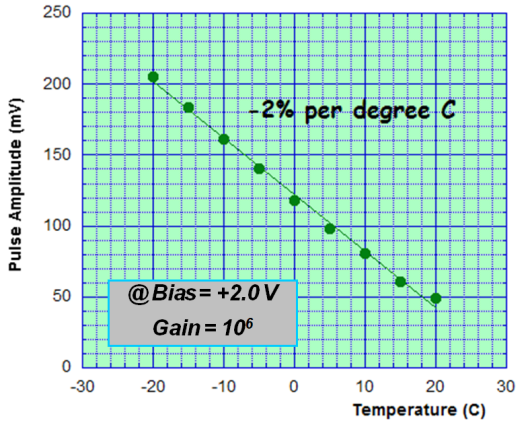

Figure 3.7: Change of pulse amplitude for the A20L sample as the temperature of the chip is changed for an overbias value of 2 volts. The 2% per degree effect is indicative of the importance of temperature control of the device during operation in poorly controlled environment.

something comparable to what a standard phototube would give from a plastic scintillator with decay times below 5 ns as is seen in the A20L sample. SensL is actively working to improve the decay time.

Initial dark current measurements, when compared to that of the previous set indicate that a substantial improvement ($>$ x10) has been made in lowering the noise level. It should be possible to obtain resolvable photopeaks at room temperature either with this device or perhaps one of the type A20L where the smaller pixel size and lower fill factor should give even larger improvements in lower noise levels.

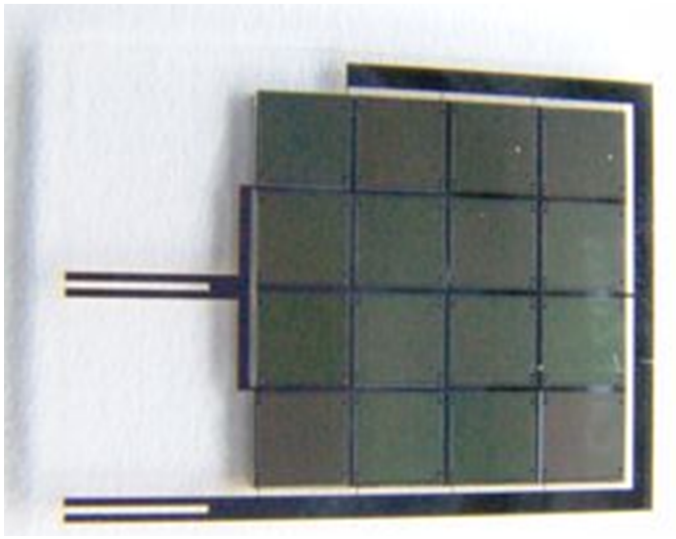

Figure 3.8: Photograph of one of the 4×4 prototype SiPM arrays made from 16 of the 3×3 mm^2 sensors of type A35H

3.3 New reference sample

The latest sample is a 1 mm^2 sample of type A20H that has incorporated trenches to reduce the crosstalk factor. The sample has produced an excellent series of spectra featuring well-resolve multiphotoelectron peaks, all recorded at room temperature. Figure 3.10 displays a series of such spectra at differing light intensities (blue LED only) and biases. Figure 3.11a) shows the resultant gain curve showing a linear relation and an overall internal gain of better than 10^6. Figure **??**b) shows the overall dark rate and contribution from the crosstalk factor. As a comparison, the first generation of devices (A20L) easily had crosstalk factors exceeding 10% at the cooled temperature of -20°C. Figure 3.12 shows a typical dark spectrum from the device showing both the single and double photoelectron peaks. The latter are due to crosstalk.

3.3.1 Gain variations in 3×3 mm^2 A35H samples

Measurements performed at the University of Regina on the present set of 4x4 pixel arrays indicate the presence of relative large variation in the gain of the pixels. The role of the layout process is being investigated as a possible cause. To provide some possible insight, the 5 individual samples were tested. Using the new A20H reference sample, the 5 A35H samples were exposed to a variety of intensities not exceeding 250 photons per mm^2 to maintain linear behavior well below any saturation level. A bias of 1.0 volts was chosen as this would approximately match the gain of the A20H sample (operated at 2.0 volts bias). (Recall that Figure 3.4 which shows the gains of the original cooled samples.) Figure 3.13 is a display of the relative outputs. (Pedestals are subtracted and all biases are relative to the breakdown voltage of the individual device.) Clearly, the devices display differing gains. As a possible cause, Figure 3.14 shows the dark currents of the differing devices with a closeup of these dark currents near the 1.0 volt bias chosen for the measurments shown on the right panel. At the qualitative level, there is a good correlation between the dark currents and the hierarchy of gains, excepting for sample 10 which, along with sample 6, has the highest dark current, but which also has the lowest relative gain.

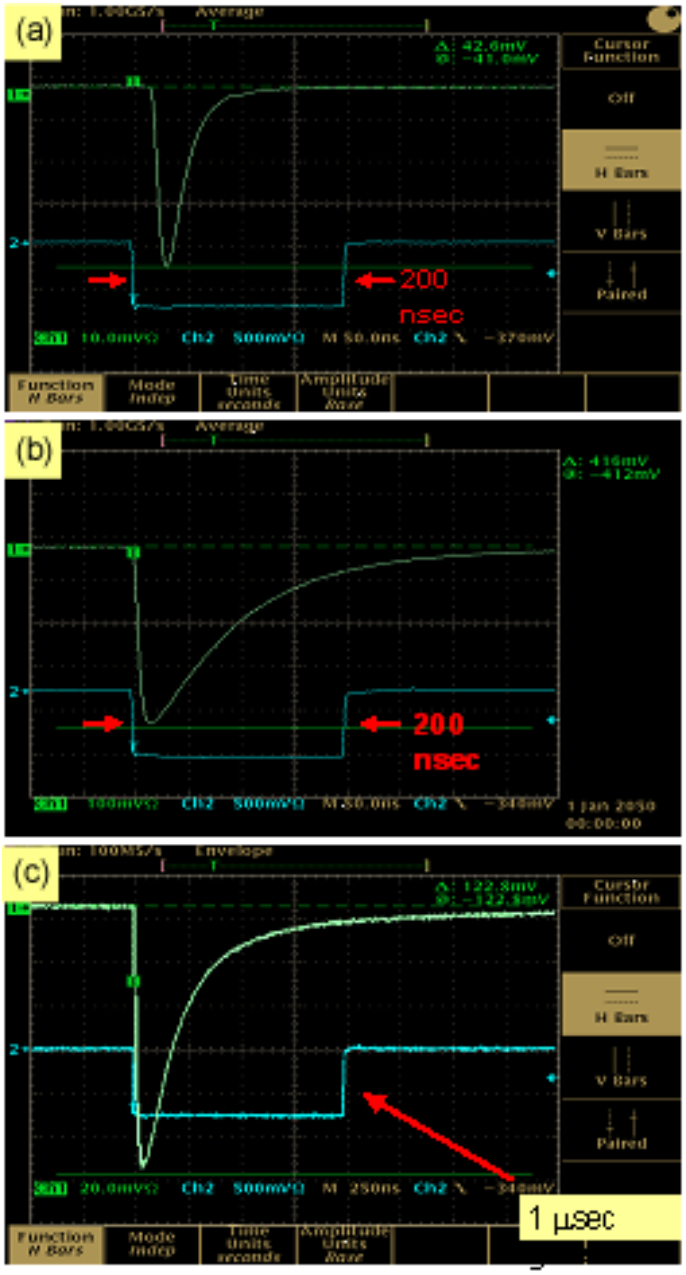

Figure 3.9: Comparison of pulse shapes of (a) A20L, (b) A35H, and (c) A35H 4×4 array when pulses with a fast blue LED.

A photograph (Figure 3.15) showing the two samples (6 and 10) shows what is probably the cause of this discrepancy. While sample 6 has a clean surface, sample 10 has various deposits which must be scattering or absorbing the incoming light. So the correlation between relative gain and dark current still stands.

Figure 3.16 shows the output of one of the samples as a function of a small change in bias ($\pm$ 0.15 volts). The overal large change illustrates the need for a tight control on the breakdown voltage among the pixels

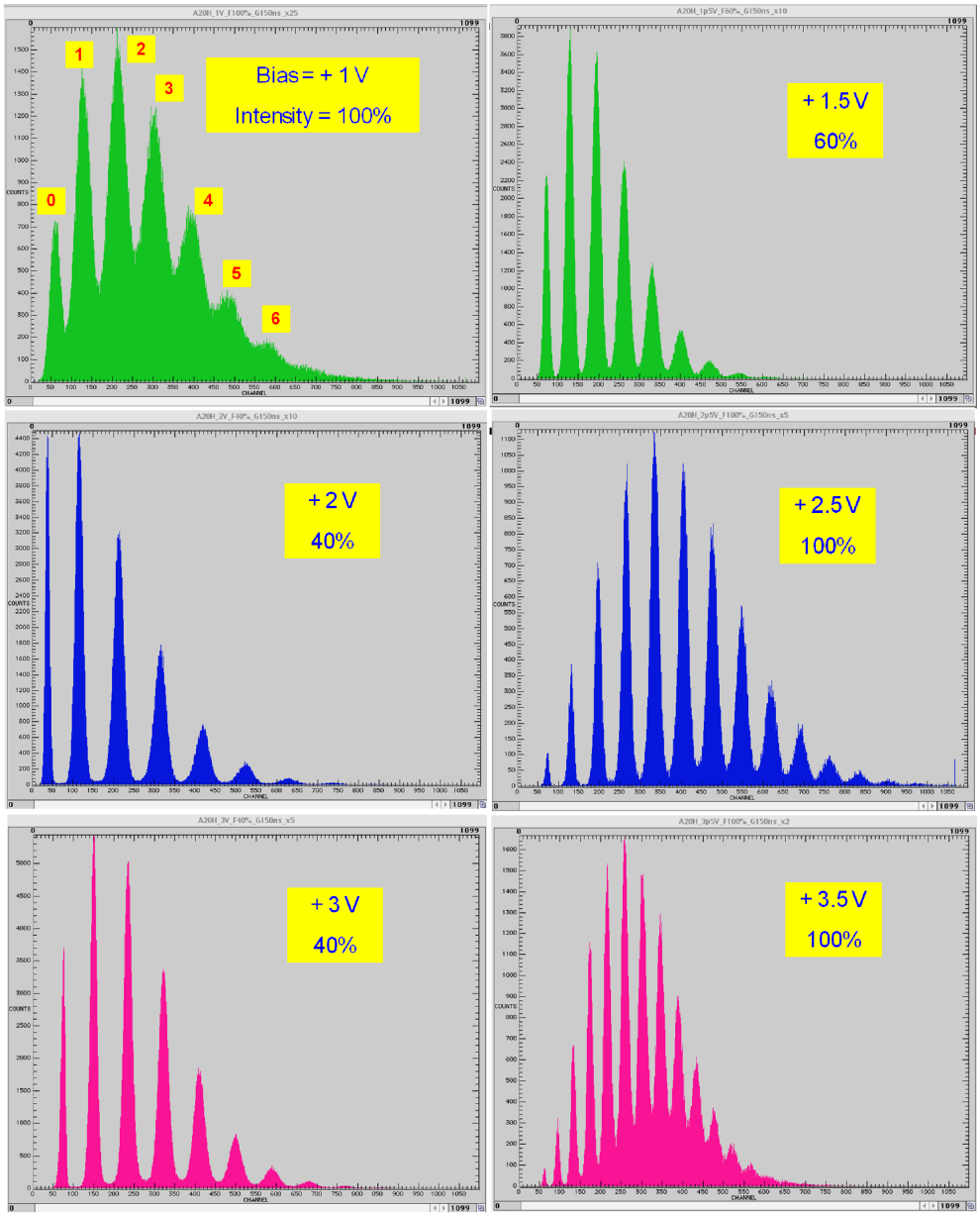

Figure 3.10: ADC spectra of new trenched A20H sample showing the well resolved multiphotopeaks at a variety of intensities and overbiases, all taken at room temperature. This is now the reference device for comparison measurements.

of an array. The 5 samples here had a range of breakdown voltages from 27.15 to 27.35 volts. Such a range (0.2 volts) would result in a large variation in the gain of the individual tiles in the array for some given average breakdown voltage.

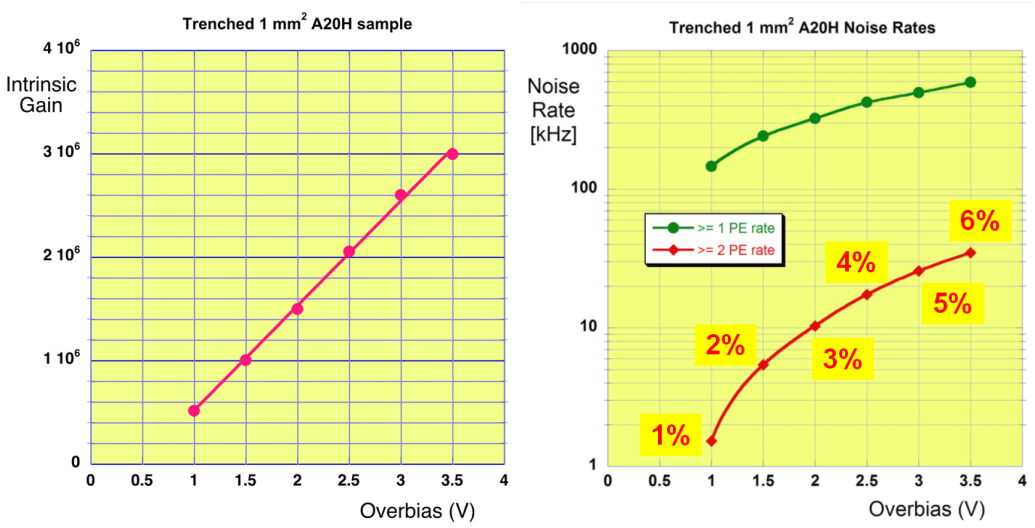

Figure 3.11: *Left panel:* a) Linear gain data for the A20H sample. *Right panel:* b) Dark rate data for the A20H sample showing the relative contribution from crosstalk to the overall dark rate.

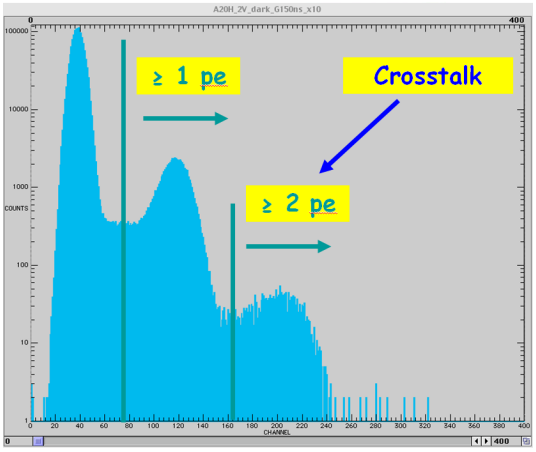

Figure 3.12: Dark noise spectrum for A20H sample showing the dark noise ($\geq$ 1 pe) and the contribution of the crosstalk factor ($\geq$ 2 pe)

3.4 Glass-mounted SiPM-array tests at the University of Regina

GlueX received five arrays from SensL, labeled G2-G6. G5 was sent to JLab and the other four were tested at the U of Regina. The testing consisted of several phases. First, the four arrays were connected to a pico-ammeter, that provided both stable reverse bias and a precision current measurement, and their IV-curves were mapped out. Then the arrays were illuminated with a green SciFi (BCF-20) that was excited by a pico-second laser (PicoQuant) at 380 nm. The SciFi had SMA connectors on both ends to match the connectors to the laser and the custom-made alignment jig. This mapped out the response of the individual cells in each array. The "surviving" arrays were then tested with several sources and BCF-20 fibers – as well as with the use of Module 2 exposed to cosmic rays using the light-guide-WC system. The results are reported in the corresponding sections below. This report starts with the global problems encountered while

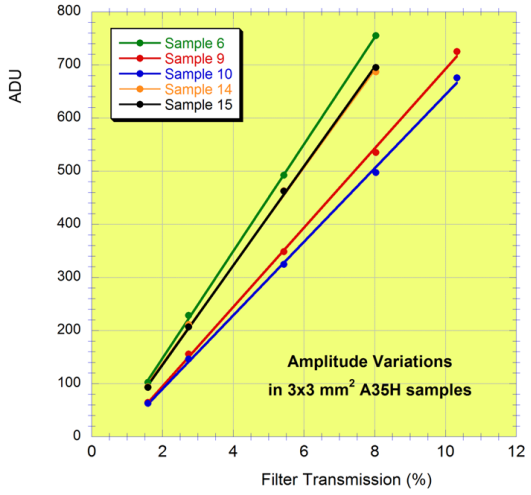

Figure 3.13: Outputs of A35H samples for same light intensity and overbias setting.

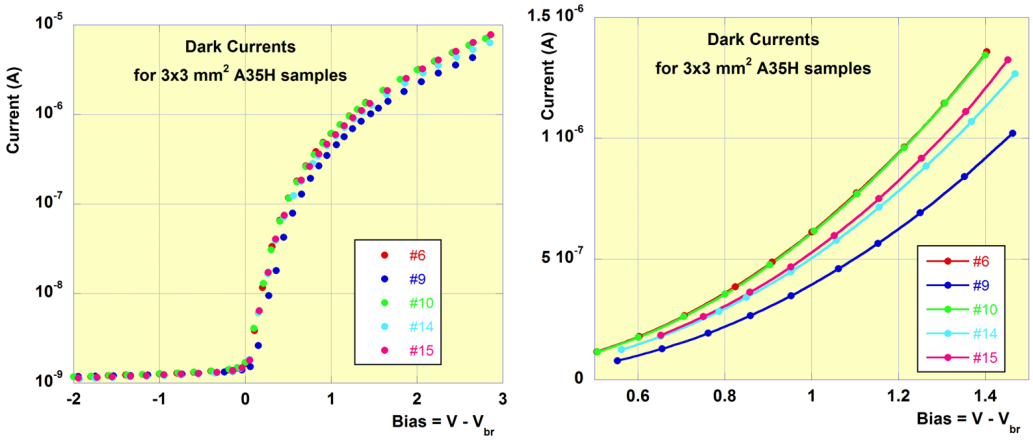

Figure 3.14: *Left panel:* a) Dark currents for A35H samples. *Right panel:* b) Closeup of the dark currents of the A35H samples near the 1.0 volt overbias and set on a linear scale to illustrate the differences and show the qualitative correlation between the sample outputs and the dark currents. Note the exceptional case of sample 10 which has a high dark current, but a low output in Figure 3.13.

testing the arrays.

3.4.1 Hardware problems

Several problems were encountered during the initial series of tests. The electronic circuits were unshielded and the connections to wire leads to the glas printed circuit board were not very robust. The connections were fixed by soldering wire leads to the board. However, the unshielded electronics were particularly susceptible to noise pick-up from various RF sources and limited the conclusions from the testing. A more detailed reporting of "noise problems" is given in Sections 3.4.3 and 3.5, below. These problems, however, have been addressed in the latest versions of the arrays that now come as integrated units with SMA and/or Molex

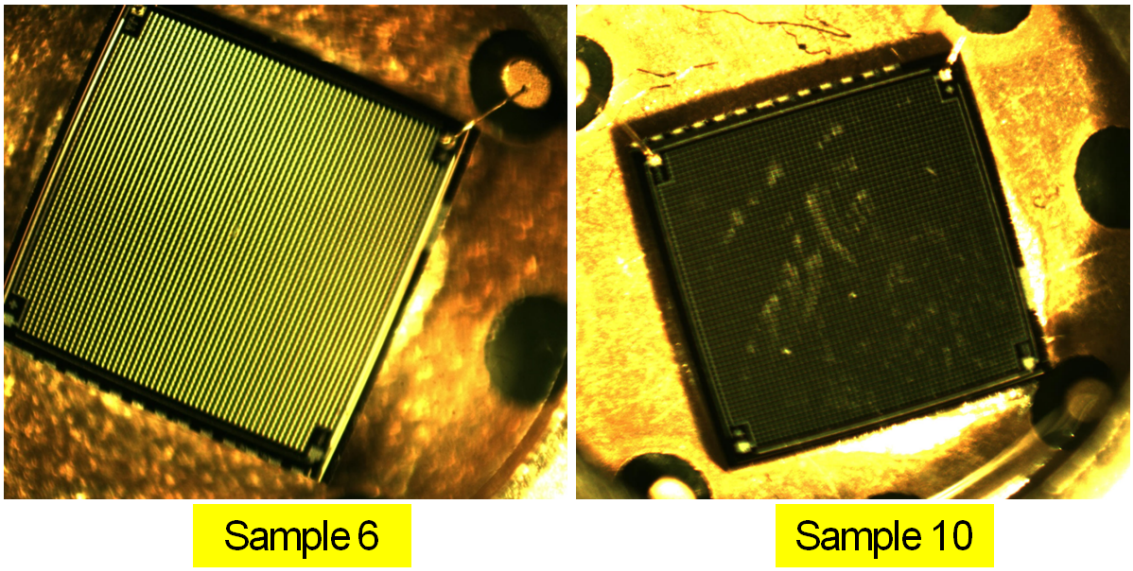

Figure 3.15: Photographs of the samples 6 and 10 which both have the highest dark current while sample 10 shows the smallest relative output. The photograph clearly shows deposits on sample 10 which could degrade its performance.

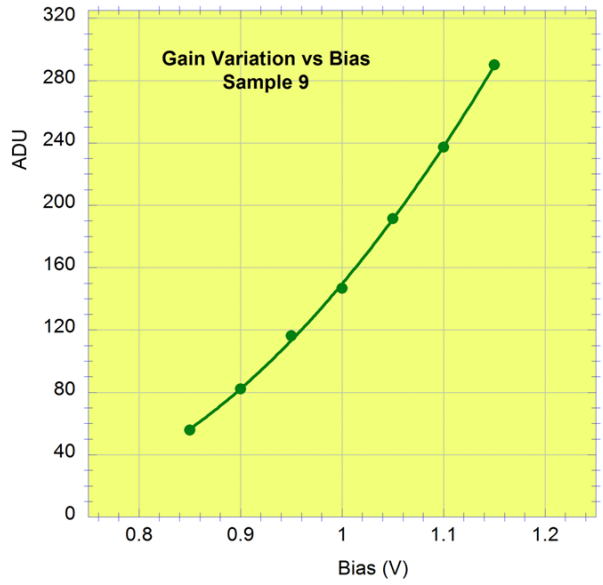

Figure 3.16: Significant changes in output as a function of small changes in overbias illustrate the need for close monitoring of the relative breakdown voltage among elements of a SiPM array.

terminals for all cabling requirements.

3.4.2 Testing results

The IV curves of the four arrays remaining at the University of Regina are shown in Figure 3.17. One can notice that G6 has a different response than the other three and that G2 and G6 have significantly higher dark current above the breakdown voltage than G3 and G4. A further investigation, of the region around the breakdown voltage, displays an unusual behaviour for G2 and G6 and this is shown in Figure 3.17. Both G2 and G6, and more so the latter, exhibit multiple break down steps above the more or less common break down voltage of ∼27.3 V. Soon after these measurements were made, G4 ceased to exhibit any signs of life and we still have not been able to diagnose the problem.

The response of each individual cell – in the three remaining functional arrays – was probed by the use of UV laser light at 380 nm, exciting a short length of BCF-20 fast green SciFi that illuminated each cell in the arrays. The SciFi was terminated with one SMA connector at each end. One end of the SciFi strand was connected to the end of the PicoQuant laser that is equipped with a fiber transporting the UV light. The fiber is also SMA terminated so the laser-to-BCF-20 connection is via a SMA barrel feed-through. The other SMA-equipped end of the BCF-20 fiber was inserted in a specially designed and machined jig that secured the SMA connector and allowed the illumination of each cell in the array. The jig and its various views are shown in Figure 3.18. The SMA connector was tightly fitted to one of the 16 holes drilled in the black (opaque) plastic alignment jig. In the center of each SMA-sized hole, a 1 mm diameter hole was drilled through and through, collimating and directing the scintillation light from the SciFi into the center of each cell, thus preventing cross talk among cells. It should be noted that, since the array was summed electronically, there was no method to actually determine the cross talk, if any, to neighbouring cells based on illumination of any particular cell. A newer SiPM array with a Molex multi-pin connector and individual readouts for each of the 16 cells has been shipped to JLab, and this unit will allow optical (illumination) cross talk determination.

The PicoQuant laser system was allowed to warm up for 20 minutes to stabilize the light intensity so any variations in response from cell to cell reflects variations in gain and possibly variations in aperture of the 1 mm diameter holes. The latter are very small. Also, the variation in light intensity due to the PicoQuant laser was estimated at about 2%. The results of the individual cell illumination are shown in Figure 3.19. We observe two main effects:

- The variations in gain between arrays are quite pronounced. Maximum amplitudes vary from ∼350 mV for G2, to ∼1100 mV for G3, and to ∼ 550 mV for G6.
- Variations among cells of the same array can be as large as factors of two. Such non-uniformities may be the result of variations in the connection quality of each cell or they may reflect the more worrisome variations in gain among cells due to more process-dependent fabrication methods.

3.4.3 General comments

Initial testing of G3 with a bundle of 20 BCF-20 fibers (each 15 cm long) – excited by a ^{90}Sr electron source – resulted in very clean pulses of ∼140 mV amplitude at +1.8 V. The pulses observed without a source were ∼ 23 mV. Assuming the latter to be representative of the one photoelectron-dominated dark rate, the source-associated signal would indicate 5-6 photo-electrons, consistent with prior measurements of a green SciFi-SiPM combination. Subsequent measurements, however, revealed a significant noise problem

that degraded the performance. This can be seen in the left panel of Figure 3.20, taken with G6 at +1.8 V. The noise does not appear to originate in the SiPM-array and it is electronic in origin.

When the oscilloscope trigger is provided by a vacuum PMT, while the BCF-20 bundle was exposed to a ^{90}Sr source, the SiPM-array exhibits a clear signal but the noise still dominates the trace, as is seen in the right panel Figure 3.20.

When initially connected to the BCAL-mounted light guide and after taking cosmic ray data under such conditions, the resulting pedestal of the ADC was very broad and masked any cosmic ray ADC signatures. The problem was traced to a very noisy power outlet source in the lab but, as this is written, its not clear whether the power line transfers the noise of any large motor on the line or some other effects are playing a role. We are also investigating the possibility that the exposed array and wires pick up RF noise from sources, such as lasers operating near by. However, when a clean power line was found, the signals from the cosmic ray energy deposition in the 2 cm-thick Pb-SciFi matrix (equivalent to 9.5 mm of scintillator) resulted to traces on the oscilloscope returning to the original clean configuration stated above.

3.5 Cosmic Ray Testing and Results

This section describes the cosmic ray testing of the SiPM-arrays, the first ever such report for lager area SiPMs.

The experimental set-up: Module 2, constructed with a combination of BCF-20 and PoliHiTech fast green and blue SciFis, respectively, has been our standard cosmic ray test bed. The trigger and event timing is provided by a $2.54 \times 2.54 \times 5$ cm^3 (W x H x L) plastic scintillator on the top of the module. It is movable along the module length and it therefore defines the event location for extraction of attenuation length. Below the module - and directly underneath the location of the trigger counter - is another scintillator counter (paddle) and the coincidence between the trigger and the paddle counter defines the cosmic ray event traversing the module. Below the paddle, and aligned with the small trigger counter, is a Cherenkov counter that uses a standard 4.1 cm diameter by 13 cm long Plexiglas light guide as the Cherenkov medium, viewed head-on by a Burle 8575 PMT. The Cherenkov counter is interrogated off-line to further collimate the muon trajectory and to assure that the event was a muon that has gone perpendicularly through 20 cm of SciFi/Pb/Epoxy matrix, thus eliminating any associated showers due to muon interaction with the module material.

The module is further instrumented with two Burle 8575 - or equivalent - PMTs viewing the bottom (blue) fibers. They are aligned so that their light-guides view the same volume of blue SciFis. Above them, and viewing the green BCF-20 SciFis. are two photo-sensors, one an EMI green sensitive PMT and the other either another EMI or, in this case, the SiPM array. Both are aligned to view the same volume of SciFis and are also aligned with all the other counters. The light guides of the three PMTs and the SiPM array are the light guide-Winston Cone assemblies we plan to employ for the read-out of the inner BCAL layers. The collection area is 2×2 cm^2 on the module side while the exit area is circular with a diameter of 1.26 cm ($\sim$1.25 cm^2). The light guides are coupled to the module with optical grease and the same is used to couple the PMTs and the SiPM array to the Winston Cone.

Cosmic ray data analysis: The average number of photoelectrons measured by the PMTs reading out the blue SciFis was ∼13, with the trigger in middle of Module 2. For the EMI PMTs and BCF-20 combination, the number was ∼9 photoelectrons. The lower Q.E. of the EMI PMTs is reflected in these numbers. Figure 3.21 shows the spectra obtained from the SiPM array with the event trigger as described above, but without the Cherenkov in the trigger.

The pedestal in the top panel is obtained by demanding that no event was associated with the EMI PMT on the other side, no event recorded by the two PMTs viewing the blue SciFis and no Cherenkov signal. The events outside the pedestal may be due to the leakage of actual events and/or some part of the pedestal "tail". The pedestal of the green sensitive EMI PMT on the other end - viewing the same volume of BCF-20 SciFis as the SiPM array also shows a similar "tail". The wide gate (∼500 ns) necessary to integrate the broad SiPM pulse makes such leakage more likely than with the normal 60 ns gates when dealing with PMT signals. The width of the pedestal is $\sigma \approx$14 channels and it is also much wider than that of the PMT on the other side that has $\sigma \approx$5 channels (EMI results are not shown).

The width of the pedestal was found to be very sensitive to the quality of the power supplied to the SiPM array. By using the Keithley picoammeter to supply the operating power and by changing the power line within the lab, the width of the pedestal decreased by approximately a factor of 2.5! We do not have enough power supplies – to the quality of the Keithley – to use for both the SiPM and its pre-amp (∼29 V and +5 V and -5 V, respectively) and we cannot investigate at this time the possible negative effect our cheaper and less stable power supplies are having on the pre-amp. Nevertheless, it is clear that the quality of the power supplied to the board plays a major role in the quality of the output signal obtained.

The middle panel in Figure 3.21 shows the ADC spectrum of the G3 SiPM array at +2 V (29.4 V) in coincidence with the trigger counters and the EMI PMT viewing the same volume of BCF-20 fibers on the other side of Module 2. Amplitude cuts have been placed on the EMI and the trigger counters to assure MIP energy deposition. The number of events under the pedestal reflect a combination of "non-events" or gates without a signal above noise and leakage from low amplitude pulses.

The bottom panel is the result of the subtraction of the pedestal based on the fit shown in the top panel. The purpose of this exercise is to ascertain qualitatively whether the spectrum can be separated from the pedestal, as a proof of principle, rather than aiming at a precise method of pedestal subtraction. The ADC spectra from G3 are quite broad. As a comparison, the EMI PMT width of its ADC spectrum is a factor of 2 narrower. We believe that the width of the G3 is dominated by the variation in gains shown in Figure 3.19. We will attempt to correct for this variation assuming a uniform light distribution incident on the array and this report will be updated accordingly. As it is now, its not possible to extract the number of photoelectrons from this measurement.

3.5.1 The effect of the elecronics board on performance

When the G6 SiPM array was tested under identical conditions to that of the G3, above, but with a different board among the four received, the ADC spectrum obtained was quite different in appearance than the one for G3. The pedestal extends from channel zero to 400 and the separation from the signal was not possible. This can be seen in the left panel of Figure 3.22 labeled as G6+G6 amplifier. The top panel is the pedestal spectrum taken under the same conditions as that for G3 in Figure 3.21. The cosmic ray ADC data spectrum is shown in the left bottom panel. The right panels show the corresponding spectra, but this time the G6 array is coupled to the electronics board originally coupled to G3, as in Figure 3.21. In this case, G6 is responding like G3, even though its IV curve had shown these multiple breaks shown in Figure 3.17. These

observations, coupled to the sensitivity of the pedestal width to the quality of the voltage supplied to the boards, point to the important role the optimization of the electronics components and their quality play in evaluating the sensors.

References

[1] Z. Papandreou. SiPM Primer. Technical report, GlueX Collaboration, 2007. GlueX-doc-741-v2.

[2] G. Lolos. A critical review of BCAL readout options. Technical report, GlueX Collaboration, 2007. GlueX-doc-799-v1.

[3] G. Lolos. Brief review of BCAL and SiPM systems. Technical report, GlueX Collaboration, 2007. GlueX-doc-807-v1.

[4] G. Lolos. BCAL readout review 2007. Technical report, GlueX Collaboration, 2007. GlueX-doc-808-v3.

[5] G. Lolos. Brief report on SiPM array developments. Technical report, GlueX Collaboration, 2007. GlueX-doc-848-v2.

[6] C. Zorn. Notes on the latest SiPM developments. Technical report, GlueX Collaboration, 2007. GlueX-doc-899-v1.

[7] C. Zorn. SiPM Presentation at the 2007 IEEE NSS/MIC Conference. Technical report, GlueX Collaboration, 2007. GlueX-doc-913-v1.

[8] G. Lolos. Testing report of SiPM arrays under Phase I. Technical report, GlueX Collaboration, 2007. GlueX-doc-926-v4.

[9] C. Zorn. Some results with the new trenched A20H SiPM sample. Technical report, GlueX Collaboration, 2008. GlueX-doc-932-v1.

[10] C. Zorn. Tests of SensL silicon photomultiplier prototypes at Jefferson Lab. Technical report, GlueX Collaboration, 2008. GlueX-doc-961-v1.

[11] P. Buzhan et al. Silicon photomultiplier and its possible applications. *Nucl. Instrum. Meth.*, A504:48–52, 2003.

[12] C. Piemonte. A new silicon photomultiplier structure for blue light detection. *Nucl. Instrum. Meth.*, A568:224–232, 2006.

[13] V.D. Kovaltchouk et al. Comparison of a silicon photomultiplier to a traditional vacuum photomultiplier. *Nucl. Instrum. Meth.*, A538:408–415, 2005.

[14] A.N. Otte et al. A measurement of the photon detection efficiency of silicon photomultipliers. *Nucl. Instrum. Meth.*, A567:360–363, 2006.

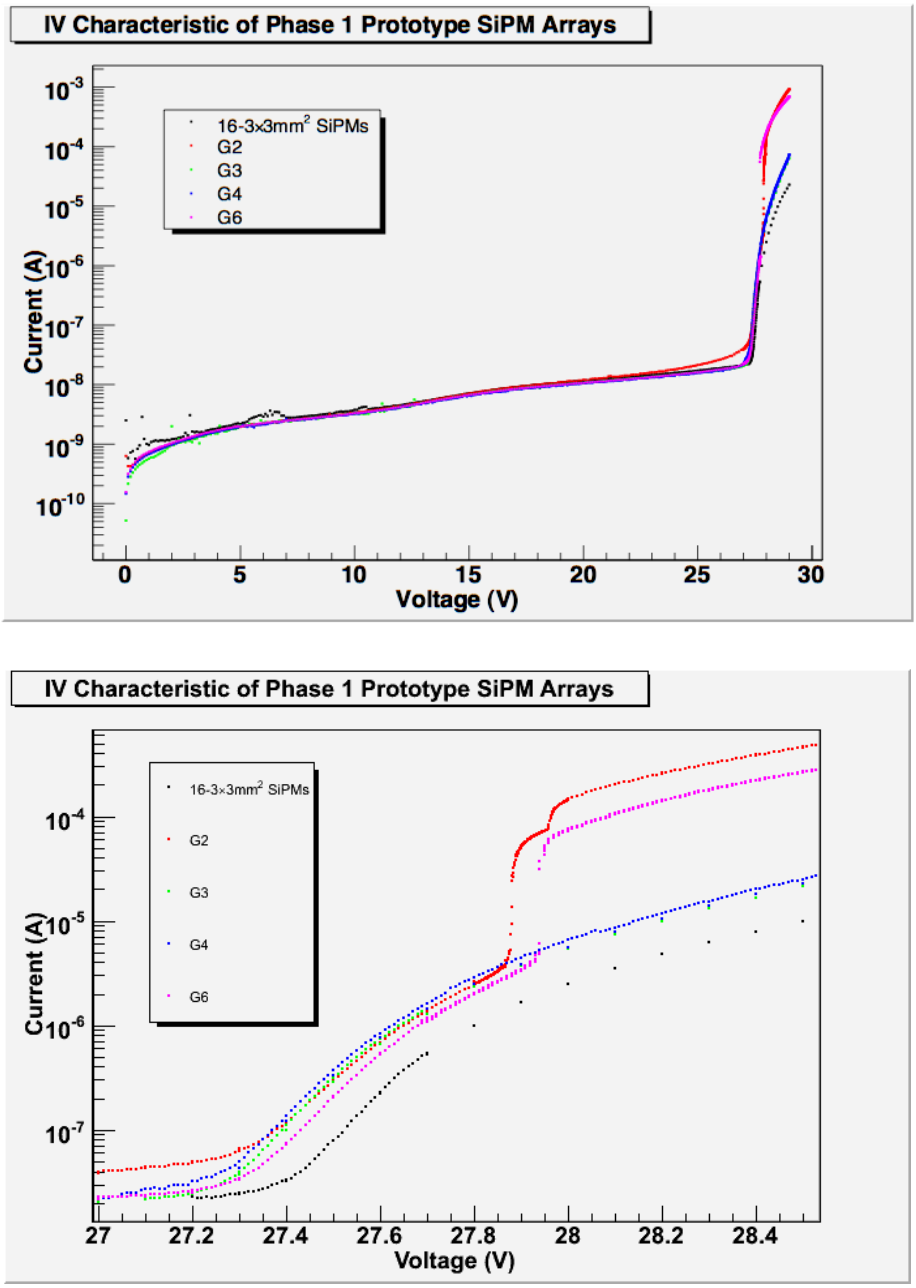

Figure 3.17: *Top panel:* The IV curves of G2, G3, G4 and G6 arrays together with the mean IV curve of the 3×3 mm^2 SiPMs, multiplied by a factor of 16, for comparison. *Bottom panel:* Close-up of the breakdown voltage region showing the abnormal behaviour of G2 and G6. Curves that displayed a uniform behaviour were sampled less frequently over a subset of their range, as shown in points spaced further apart such as for the 16 3×3 mm^2 SiPMs as well for array G3.

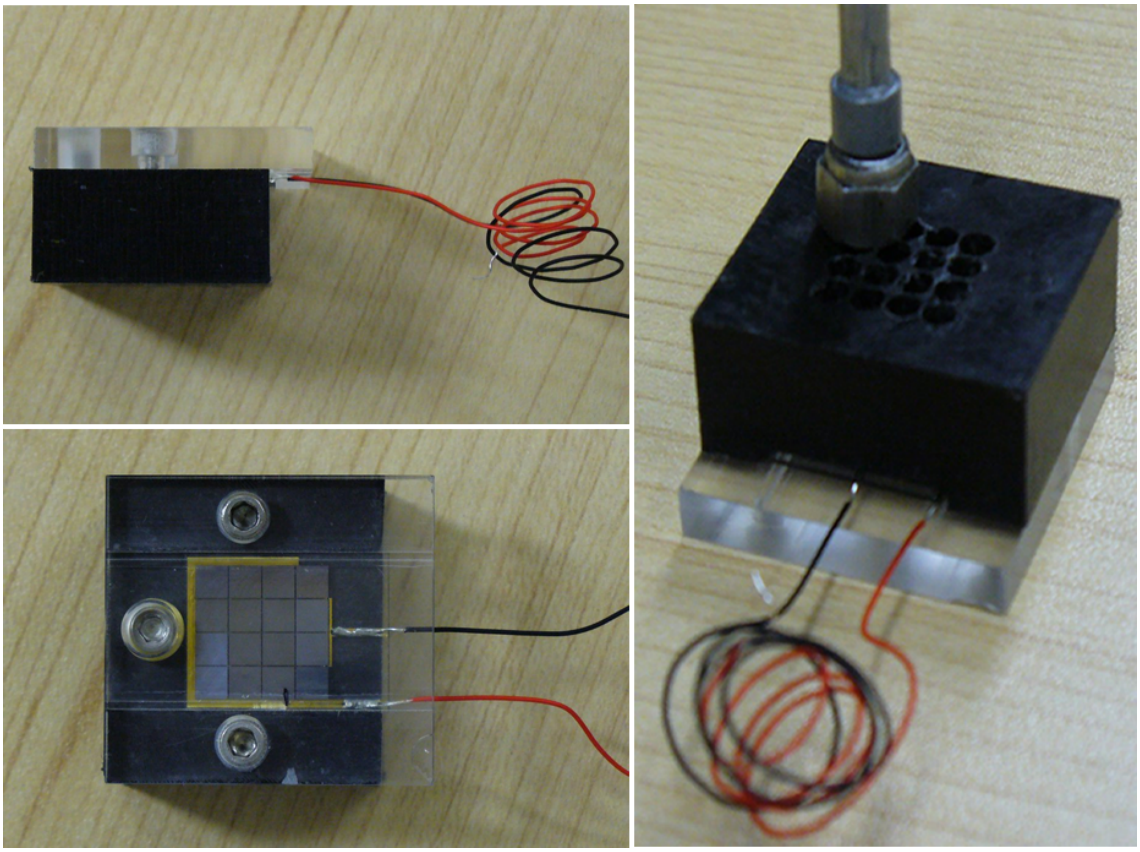

Figure 3.18: *Left top panel:* Side view of the jig consisting of two parts, the black (opaque) plastic SMA mounting and alignment part and the SiPM-array aligning clear part. *Left bottom panel:* Bottom view of the jig showing the mounted SiPM- array (non-active side showing). Each 3×3 mm^2 cell views a 1 mm diameter hole (on the other side) in the black plastic centered on the 1 mm diameter SciFi. *Right panel:* The upper side of the jig with the array mounted and the SMA connector with the BCF-20 SciFi attached to one of the holes drilled in the black plastic, in this case illuminating the cell on one corner of the array.

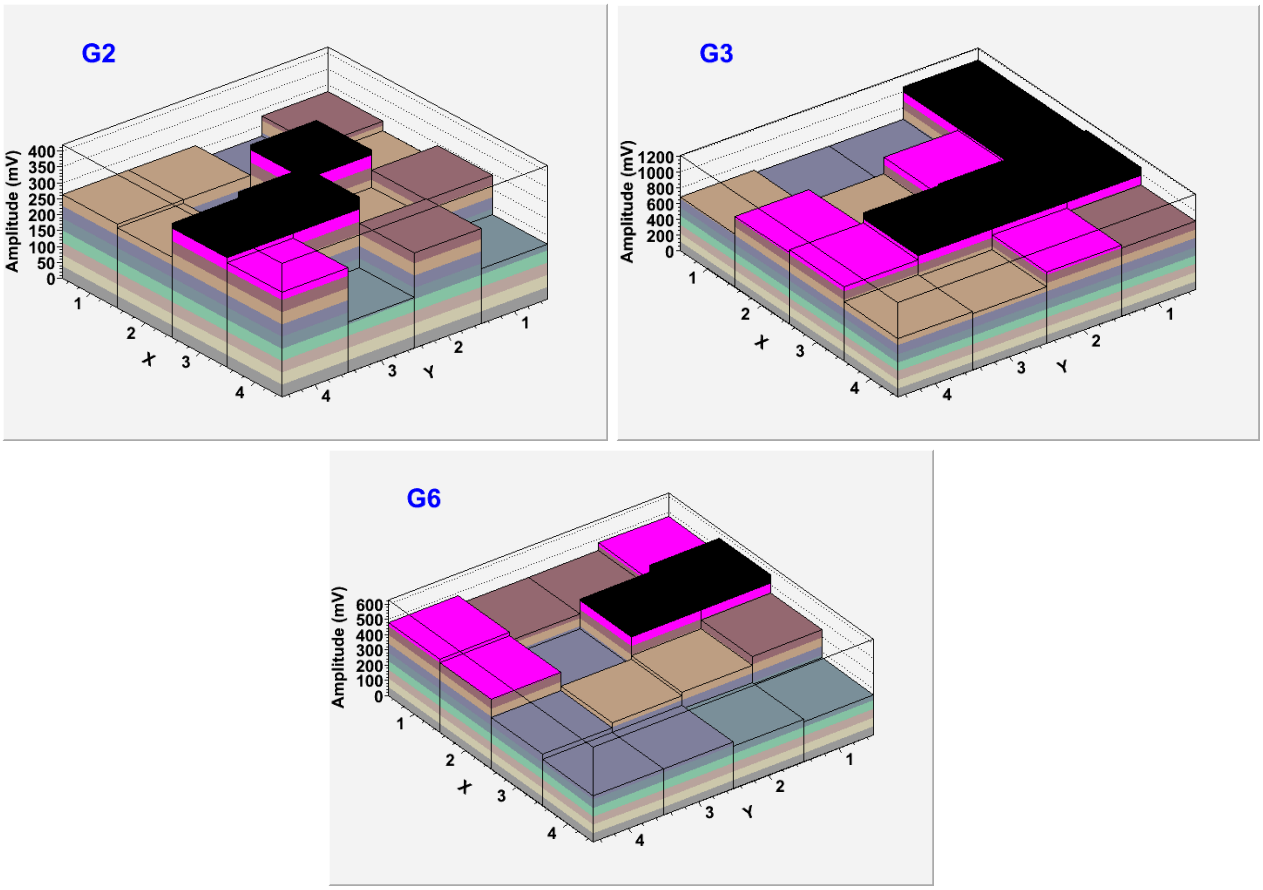

Figure 3.19: Pulse amplitude mapping across 16 cells for SiPM-arrays G2, G3 and G6.

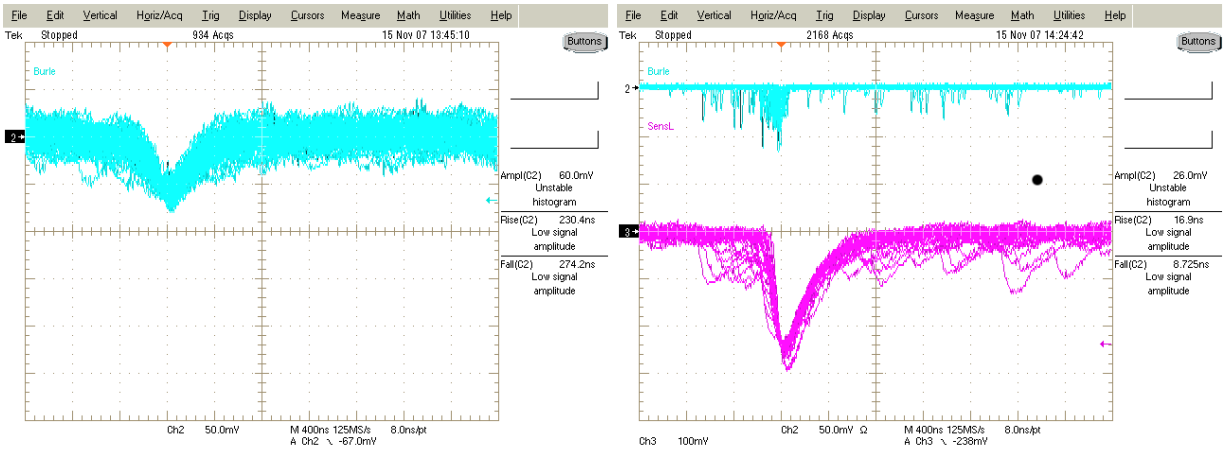

Figure 3.20: *Left panel:* Trace of G6 at +1.8 V without the ^{90}Sr source present on the bundle of BCF-20 SciFis. *Right panel:* Trace of G6 (purple) at +1.8 V with Sr-90 source present on bundle of green SciFis. The green trace is from a Burle 8575 PMT acting as the trigger. All traces are shown after the noisy power line problem was rectified.

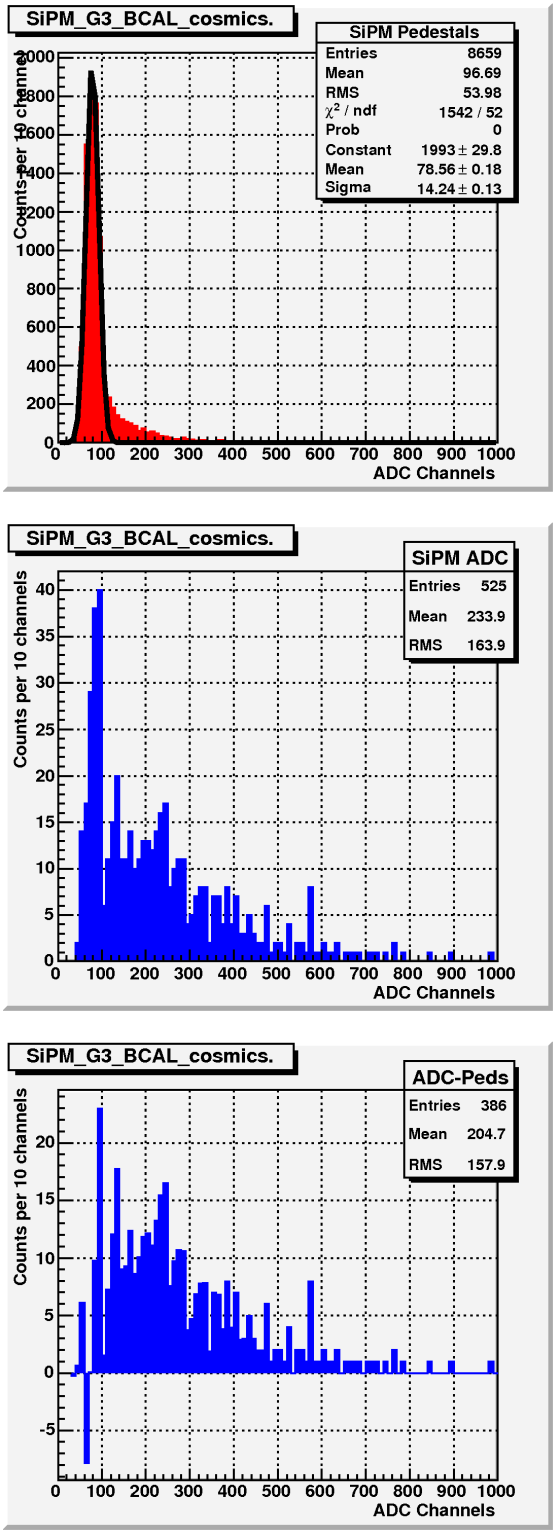

Figure 3.21: Top panel is the SiPM pedestal. Middle panel is the ADC spectrum without pedestal subtraction. Bottom panel is the result of pedestal subtraction using a fit to the shape in the top panel.

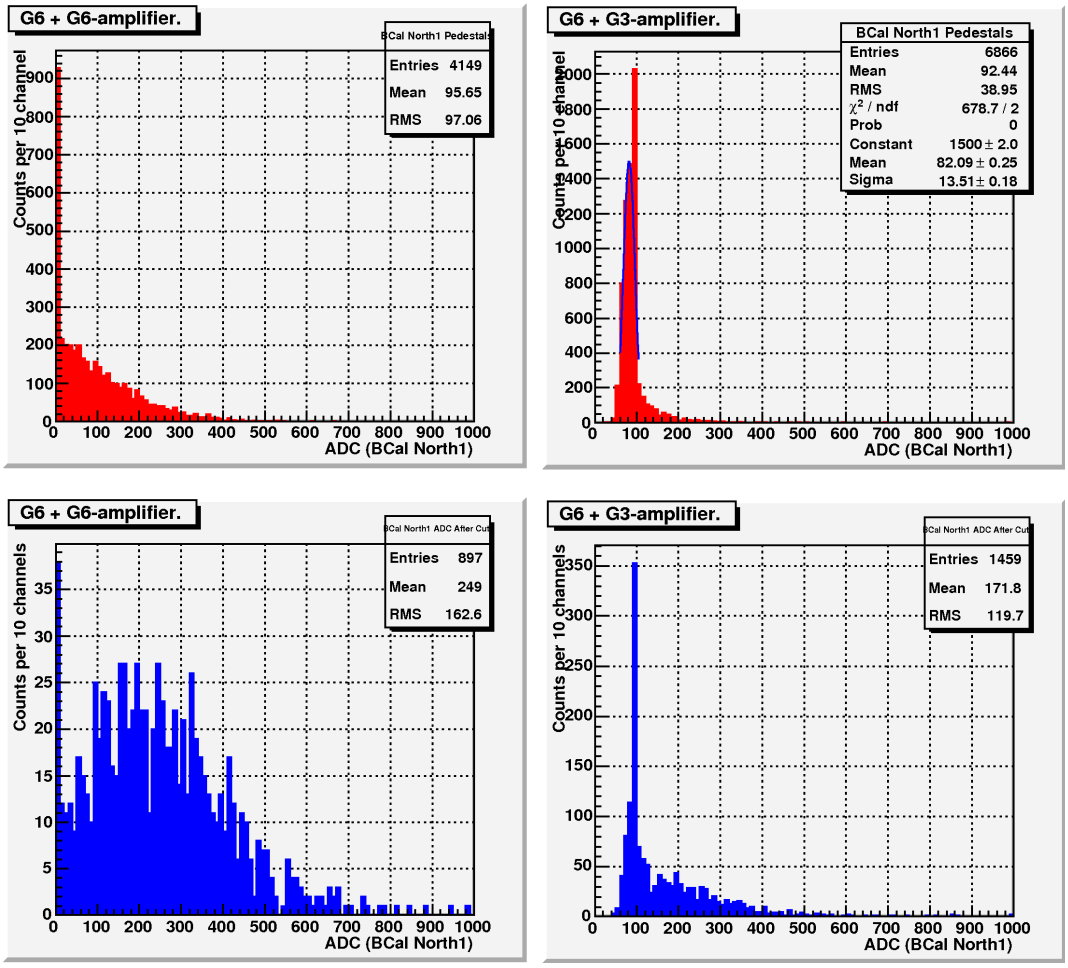

Figure 3.22: Top left panel is the SiPM pedestal with the G6 board. Top right panel is the corresponding pedestal spectrum with the G3 array coupled to the board used for the G3 data shown in Figure 3.21. Bottom panels are the corresponding cosmic ray ADC spectra taken under the same trigger conditions as that of G3 shown in Figure 3.21.